Preprints of the 21st IFAC World Congress (Virtual)
Berlin, Germany, July 12-17, 2020

In-Vehicle System Identification of an Induction Motor Loss Model ⋆

Bernhard Rolle, Oliver Sawodny *

* *Institute for System Dynamics, University of Stuttgart, Stuttgart, Germany (e-mail: rolle@isys.uni-stuttgart.de; sawodny@isys.uni-stuttgart.de).*

Abstract: The influence of induction motor model parameter deviations on field-oriented control performance has been widely investigated. Various methods have been introduced to track variations of magnetic and resistive parameters of the so called T-equivalent circuit model. Online methods on embedded systems exist and are successfully used in modern motor controls. For the use in vehicle motion control and particularly supervisory controls, however, state-of-the-art identification methods may not be applied directly, due to restricted communication interfaces or a limited amount of available measurements at sampling frequencies above the required rates. To cope with these limitations, a moddeling approach is introduced which is based on the equivalent flat system representation of the induction motor, stationary operation conditions, and the incorporation of the vehicle specific field-oriented control strategy. The inclusion of the control strategy allows for derivation of least-square error formulations which are used to identify a selection of induction motor model parameters from low frequency vehicle measurements. An experimental study demonstrates the accuracy of the proposed method and shows how effectively the introduced model can reproduce the measurment of the rms phase current and electric power.

Keywords: electric vehicles, induction motors, least-squares identification, system models.

1. INTRODUCTION

Due to low production and design costs, safety advantages in the case of fault drive operations, and very good overload capabilities, induction motors (IM) are a common choice for drivetrains of battery electric vehicles (Finken et al. [2008], Pellegrino et al. [2012]). Although the fast response rate of electric machines offer many advantages, a model-based integration into a classical automotive motion control system is challenging. Due to low electric and magnetic time constants, which govern electric motor dynamics on the scale of several kHz, high demands are exerted on the control hardware. Nevertheless, the trend towards faster and more powerful microprocessors inspires a model-based development of control functions, which for example aim for an optimized efficiency of induction motor drives (Windisch and Hofmann [2015], Rolle and Sawodny [2019]).

Model based approaches, however, strongly depend on the accuracy of the chosen model structure and its defining parameter set. Depending on the complexity and application of the model and since it is often the case in practice that the access to internal motor control functions and measurements are restricted for proprietary reasons, parameters may not be known or are difficult to obtain. Furthermore, it may be desirable to track parameter variations online by means of suitable estimation or system identification methods. There is a large volume of published studies describing different model structures and parameter estimation methods for online and offline identification of induction motors. Industrialized identification and testing procedures such as IEEE [2018] exist. A very extensive overview on identification methods with numerous references to related publications is found in Toliyat et al. [2003]. Offline identification methods often imply some special conditions on the test procedure. The method purposed by Castaldi and Tilli [2005], relies on standstill tests in which only one phase is excited. Shaw and Leeb [1999] on the other hand, obtain current and voltage measurements from transient tests and presuppose conditions on the slip frequency. Online identification methods are typically restricted to a reduced selection of model parameters. A common choice to identify the rotor time constant is the extended Kalman filter (Atkinson et al. [1991],Zai et al. [1992]). More recently Yang et al. [2017] introduced a method which identifies the rotor resistance and mutual inductance by designing a model reference adaptive system (MRAS) based on the observed rotor flux. The estimated flux is obtained by a high-order terminal slinding-mode observer (SMO) in series with a first order SMO which are shown to be robust against mismatches of the identified parameters.

The accuracy of parameter determination techniques strongly depend on the selected sampling rate of the underlying measurement. The prerequisite of electric state measurements to be at high sampling frequencies, however, makes it difficult to use state-of-the-art identification methods in a motion control systems where not all required measurements are available and where measurements are

⋆ The authors would like to thank the Daimler AG for funding this research project and for providing experimental vehicles and testing equipment.

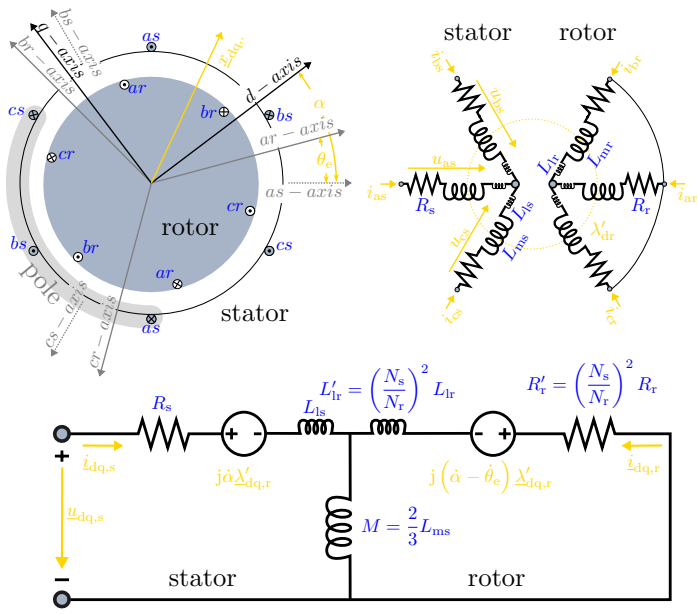

Fig. 1. Symmetrical 3-phase 2-pole induction motor (top) and T-form equivalent circuit (bottom).

sampled at considerably lower sampling frequencies. In this study, a fundamentally different approach is presented to identify a selection of IM parameters from rms current, electric power, and rotor speed measurements, as well as an accurate estimation of the rotor torque, all being available states on the internal vehicle communication bus system. The main difference compared to other methods is the moddeling approach of the measured states, which exploits the property of differential flatness and incorporates an a priori knowledge of the field oriented control strategy. This knowledge allows to establish a hypotheses on the flux level which considerably influences the magnetic parameters especially in saturation conditions. Furthermore, under the assumption of stationary operating conditions, which have proven to be reasonable for the intended use of the IM model, parameterized mappings from past measurements to the space of the modeled outputs are derived and used to identify the selected parameter set in a least-square manner. The induction motor model obtained thereby is not intended to be used in high performance motor control but rather for loss estimations.

The discussion of the proposed modeling and estimation approach is done in four sections. Section 2 provides a review on the classical modeling approach of the T-form equivalent circuit and extends this model by incorporating magnetic core losses. Based on this model, the equivalent flat system and the underlying assumptions of the parameter identification method are presented in Section 3. An experimental study, described in Section 4, demonstrates the modeling as well as the parameter estimation accuracy. Finally Section 5 summarizes the results and gives a short outlook on future work.

2. INDUCTION MOTOR MODEL

This section provides a brief summary of the modeling approach described by Krause and Thomas [1965] and Krause et al. [2013], which is used as a baseline for the following model identification.

Given a squirrel-cage motor and assuming a spatial, sinusoidal magnetomotive force in the air gap, it is convenient to express spatially distributed windings as equivalent coils. Figure 1 shows such a 3-phase 2-pole motor with identical resistance $R_{(.)}$, identical leakage inductance $L_{\mathrm{l}(.)}$, and identical self-inductance $L_{\mathrm{m}(.)}$ for both stator and rotor. The mutual coupling between stator and rotor coils is represented by the mutual inductance L_{sr}. Suffixes $_{\mathrm{s}}$ and $_{\mathrm{r}}$ either indicate stator or rotor for the respectie parameters and states. If suffixes are dropped $_{(.)}$, the corresponding relation is valid for either stator or rotor. The 2-pole motor can easily be extended to multiple poles by multiplying the expression of the rotor angle θ_{r} with the pole-pair number Z_{p}, which yields the electric rotor angle θ_{e}. The line-to-neutral voltage equations are

$$\begin{bmatrix} \boldsymbol{u}_{\mathrm{abc,s}} \\ \boldsymbol{0} \end{bmatrix} = \begin{bmatrix} \boldsymbol{R}_{\mathrm{s}} & \boldsymbol{0} \\ \boldsymbol{0} & \boldsymbol{R}_{\mathrm{r}} \end{bmatrix} \begin{bmatrix} \boldsymbol{i}_{\mathrm{abc,s}} \\ \boldsymbol{i}_{\mathrm{abc,r}} \end{bmatrix} + \frac{\mathrm{d}}{\mathrm{dt}} \begin{bmatrix} \boldsymbol{\lambda}_{\mathrm{abc,s}} \\ \boldsymbol{\lambda}_{\mathrm{abc,r}} \end{bmatrix} , \tag{1}$$

where $\boldsymbol{R}_{(.)} = \mathrm{diag}(R_{(.)}, R_{(.)}, R_{(.)})$ are block diagonal matrices containing the respective stator or rotor resistances and bold symbols indicate the vector notation of the balanced 3-phase voltage $\boldsymbol{u}_{\mathrm{abc,s}}$, current $\boldsymbol{i}_{\mathrm{abc,(.)}}$, and flux linkage $\boldsymbol{\lambda}_{\mathrm{abc,(.)}}$. For example, stator phase voltages with fundamental electrical angular frequency $\dot{\theta}_0$ and peak value $\hat{u}$ are

$$\boldsymbol{u}_{\mathrm{abc,s}} = \left[\hat{u}\cos\left(\dot{\theta}_0 t\right)\ \hat{u}\cos\left(\dot{\theta}_0 t - \tfrac{2\pi}{3}\right)\ \hat{u}\cos\left(\dot{\theta}_0 t + \tfrac{2\pi}{3}\right)\right]^T . \tag{2}$$

Within the magnetically coupled electric circuit, the flux linkages are governed by

$$\begin{bmatrix} \boldsymbol{\lambda}_{\mathrm{abc,s}} \\ \boldsymbol{\lambda}_{\mathrm{abc,r}} \end{bmatrix} = \begin{bmatrix} \boldsymbol{L}_{\mathrm{s}} & \boldsymbol{L}_{\mathrm{sr}} \\ \boldsymbol{L}_{\mathrm{sr}}^T & \boldsymbol{L}_{\mathrm{r}} \end{bmatrix} \begin{bmatrix} \boldsymbol{i}_{\mathrm{abc,s}} \\ \boldsymbol{i}_{\mathrm{abc,r}} \end{bmatrix} . \tag{3}$$

Above inductance matrices are defined as

$$\boldsymbol{L}_{(.)} = \boldsymbol{L}_{(.)}^T = \begin{bmatrix} L_{\mathrm{l}(.)} + L_{\mathrm{m}(.)} & -0.5L_{\mathrm{m}(.)} & -0.5L_{\mathrm{m}(.)} \\ \cdot & L_{\mathrm{l}(.)} + L_{\mathrm{m}(.)} & -0.5L_{\mathrm{m}(.)} \\ \cdot & \cdot & L_{\mathrm{l}(.)} + L_{\mathrm{m}(.)} \end{bmatrix} , \tag{4}$$

$$\boldsymbol{L}_{\mathrm{sr}}(\theta_{\mathrm{e}}) = \begin{bmatrix} L_{\mathrm{sr}}\cos\left(\theta_{\mathrm{e}}\right) & L_{\mathrm{sr}}\cos\left(\theta_{\mathrm{e}} + \frac{2\pi}{3}\right) & L_{\mathrm{sr}}\cos\left(\theta_{\mathrm{e}} - \frac{2\pi}{3}\right) \\ L_{\mathrm{sr}}\cos\left(\theta_{\mathrm{e}} - \frac{2\pi}{3}\right) & L_{\mathrm{sr}}\cos\left(\theta_{\mathrm{e}}\right) & L_{\mathrm{sr}}\cos\left(\theta_{\mathrm{e}} + \frac{2\pi}{3}\right) \\ L_{\mathrm{sr}}\cos\left(\theta_{\mathrm{e}} + \frac{2\pi}{3}\right) & L_{\mathrm{sr}}\cos\left(\theta_{\mathrm{e}} - \frac{2\pi}{3}\right) & L_{\mathrm{sr}}\cos\left(\theta_{\mathrm{e}}\right) \end{bmatrix} . \tag{5}$$

The undesirable variation of (5) with respect to the displacement angle θ_{e} can be eliminated by the complex space vector transformation

$$\begin{aligned} \underline{x}_{\mathrm{dq,s}} &= \frac{2}{3}\left(x_{\mathrm{as}} + x_{\mathrm{bs}}\,\mathrm{e}^{\mathrm{j}\,2\pi/3} + x_{\mathrm{cs}}\,\mathrm{e}^{-\mathrm{j}\,2\pi/3}\right)\mathrm{e}^{-\mathrm{j}\,\alpha} \\ &= x_{\mathrm{ds}} + \mathrm{j}\,x_{\mathrm{qs}} , \end{aligned} \tag{6}$$

$$\begin{aligned} \underline{x}_{\mathrm{dq,r}} &= \frac{2}{3}\left(x_{\mathrm{ar}} + x_{\mathrm{br}}\,\mathrm{e}^{\mathrm{j}\,2\pi/3} + x_{\mathrm{cr}}\,\mathrm{e}^{-\mathrm{j}\,2\pi/3}\right)\mathrm{e}^{-\mathrm{j}(\alpha-\theta_{\mathrm{e}})} \\ &= x_{\mathrm{dr}} + \mathrm{j}\,x_{\mathrm{qr}} , \end{aligned} \tag{7}$$

where x either denotes a current, voltage, or flux linkage state. As shown in Fig. 1, the position of the new reference frame real, or direct, axis in relation to phase a of the stationary stator reference frame is defined by α. The factor $2/3$ is chosen so that the magnitude of the space vector $|\underline{x}_{(.)}|$ is equal to the peak value of the balanced state $\hat{x}_{(.)}$. For a further simplification of the voltage and flux equations it is convenient to relate all rotor variables to the stator windings by the appropriate turns ratio

$$\underline{\lambda}'_{\mathrm{dq,r}} = \frac{N_{\mathrm{s}}}{N_{\mathrm{r}}}\underline{\lambda}_{\mathrm{dq,r}} , \ \underline{u}'_{\mathrm{dq,r}} = \frac{N_{\mathrm{s}}}{N_{\mathrm{r}}}\underline{u}_{\mathrm{dq,r}} , \ \underline{i}'_{\mathrm{dq,r}} = \frac{N_{\mathrm{r}}}{N_{\mathrm{s}}}\underline{i}_{\mathrm{dq,r}} , \tag{8}$$

and by using the following definitions

$$R'_{\mathrm{r}} = \left(\frac{N_{\mathrm{s}}}{N_{\mathrm{r}}}\right)^2 R_{\mathrm{r}}\,,\ L'_{\mathrm{lr}} = \left(\frac{N_{\mathrm{s}}}{N_{\mathrm{r}}}\right)^2 L_{\mathrm{lr}}\,,\ M = \frac{3}{2}L_{\mathrm{ms}}\,. \quad (9)$$

Altogether, this yields the T-form equivalent circuit equations

$$\underline{u}_{\mathrm{dq,s}} = R_{\mathrm{s}}\underline{i}_{\mathrm{dq,s}} + \mathrm{j}\,\dot{\alpha}\underline{\lambda}_{\mathrm{dq,s}} + \frac{\mathrm{d}\,\underline{\lambda}_{\mathrm{dq,s}}}{\mathrm{dt}}\,, \quad (10)$$

$$0 = R'_{\mathrm{r}}\underline{i}'_{\mathrm{dq,r}} + \mathrm{j}\left(\dot{\alpha} - \dot{\theta}_{\mathrm{e}}\right)\underline{\lambda}'_{\mathrm{dq,r}} + \frac{\mathrm{d}\,\underline{\lambda}'_{\mathrm{dq,r}}}{\mathrm{dt}}\,, \quad (11)$$

$$\underline{\lambda}_{\mathrm{dq,s}} = \underbrace{(L_{\mathrm{ls}} + M)}_{=L_{\mathrm{s}}}\underline{i}_{\mathrm{dq,s}} + M\underline{i}'_{\mathrm{dq,r}}\,, \quad (12)$$

$$\underline{\lambda}'_{\mathrm{dq,r}} = \underbrace{(L'_{\mathrm{lr}} + M)}_{=L_{\mathrm{r}}}\underline{i}'_{\mathrm{dq,r}} + M\underline{i}_{\mathrm{dq,s}}\,. \quad (13)$$

In the literature there are various representations of the voltage and flux equations (10)-(13) depending on the choice of the reference frame and the system states. The following section makes use of the reference frame which synchronously rotates with the rotor flux linkage λ'_{dr} at a reference frame speed of

$$\dot{\alpha} = \frac{MR'_{\mathrm{r}}}{L_{\mathrm{r}}}\frac{i_{\mathrm{qs}}}{\lambda'_{\mathrm{dr}}} + \dot{\theta}_{\mathrm{e}}\,, \quad (14)$$

which results in $\lambda'_{\mathrm{qr}} = \dot{\lambda}'_{\mathrm{qr}} = 0$. Choosing the stator currents and rotor flux linkages as state variables, the resulting IM model equations are

$$\dot{i}_{\mathrm{ds}} = -\frac{i_{\mathrm{ds}}}{T_{\mathrm{c}}} + \dot{\theta}_{\mathrm{e}}i_{\mathrm{qs}} + \frac{M}{T_{\mathrm{r}}}\left(\frac{i_{\mathrm{qs}}^2}{\lambda'_{\mathrm{dr}}} + \frac{\lambda'_{\mathrm{dr}}}{\sigma L_{\mathrm{r}}L_{\mathrm{s}}}\right) + \frac{u_{\mathrm{ds}}}{\sigma L_{\mathrm{s}}}\,, \quad (15)$$

$$\dot{i}_{\mathrm{qs}} = -\frac{i_{\mathrm{qs}}}{T_{\mathrm{c}}} - \dot{\theta}_{\mathrm{e}}i_{\mathrm{ds}} - \frac{M}{T_{\mathrm{r}}}\left(\frac{i_{\mathrm{qs}}i_{\mathrm{ds}}}{\lambda'_{\mathrm{dr}}} + \dot{\theta}_{\mathrm{e}}T_{\mathrm{r}}\frac{\lambda'_{\mathrm{dr}}}{\sigma L_{\mathrm{r}}L_{\mathrm{s}}}\right) + \frac{u_{\mathrm{qs}}}{\sigma L_{\mathrm{s}}}\,, \quad (16)$$

$$\dot{\lambda}'_{\mathrm{dr}} = -\frac{\lambda'_{\mathrm{dr}}}{T_{\mathrm{r}}} + \frac{M}{T_{\mathrm{r}}}i_{\mathrm{ds}}\,, \quad (17)$$

where the rotor time constant T_{r}, the current time constant T_{c}, and the leakage coefficient σ are defined as

$$T_{\mathrm{r}} = \frac{L_{\mathrm{r}}}{R'_{\mathrm{r}}}\,,\ T_{\mathrm{c}} = \frac{\sigma L_{\mathrm{r}}L_{\mathrm{s}}}{L_{\mathrm{r}}R_{\mathrm{s}} + (1-\sigma)L_{\mathrm{s}}R'_{\mathrm{r}}}\,,\ \sigma = 1 - \frac{M^2}{L_{\mathrm{r}}L_{\mathrm{s}}}\,. \quad (18)$$

As pointed out by Pellegrino et al. [2012], an IM used in a vehicle drivetrain may suffer from high iron or core losses P_{cl}, which contribute to hysteresis losses and eddy currents. The former is proportional to the electrical angular frequency and the square value of the linking air gap flux $\Phi_{\mathrm{m}} = \Phi_{\mathrm{s}} + \Phi_{\mathrm{r}}$ according to the proportionality factor k_{h}. The latter is proportional to the square value of the angular frequency and Φ_{m}^2 with the proportionality factor k_{e}. Following the approach in Lim and Nam [2004], stator and rotor iron losses can be approximated by

$$P_{\mathrm{cl,s}} = \left(k_{\mathrm{h}}\dot{\theta}_0 + k_{\mathrm{e}}\dot{\theta}_0^2\right)\Phi_{\mathrm{m}}^2 \simeq \frac{\dot{\theta}_0^2\Phi_{\mathrm{m}}^2}{R_{\mathrm{fe}}}\,,\ P_{\mathrm{cl,r}} \simeq \frac{\dot{\theta}_{\mathrm{s}}^2\Phi_{\mathrm{m}}^2}{R_{\mathrm{fe}}}\,, \quad (19)$$

where $\dot{\theta}_{\mathrm{s}} = \dot{\theta}_0 - \dot{\theta}_{\mathrm{e}}$ is the slip frequency and R_{fe} is the core loss resistance. Due to small slip frequencies in nominal operation, the rotor core loss is very small compared to the stator core loss. The overall core loss can thus be further approximated by

$$P_{\mathrm{cl}} = \frac{3}{2}\frac{\left(\dot{\theta}_0 M\right)^2}{R_{\mathrm{fe}}}i_{\mathrm{ds}}^2\,. \quad (20)$$

In summary, the T-form IM model equations are given by (15)-(17). These are well suited for performance studies of IM drives in vehicle applications. For efficiency analyses, it is further recommended to account for iron losses approximated in (20). The defining parameter set is

$$p_{\mathrm{IM}} = \{Z_{\mathrm{p}}, R_{\mathrm{s}}, R'_{\mathrm{r}}, L_{\mathrm{ls}}, L'_{\mathrm{lr}}, M, R_{\mathrm{fe}}\}\,. \quad (21)$$

Figure 1 shows how these parameters, with the exception of R_{fe}, are related to the 3-phase 2-pole model.

3. SYSTEM IDENTIFICATION

The choice of a model structure and its defining parameter set are the most important steps in the system identification procedure, Ljung [2009]. Furthermore, as done by Besançon et al. [2001], it is important to analyse whether the chosen model structure allows for the structural identifiability of the involved parameter. Determination of the best model depends on the available measurement data and the performance of the model when it attempts to reproduce the measured data. The identification methods, mentioned in Section 1, all require measurements of the stator phase voltages or stator phase currents at high sampling frequencies. These are, however, not available for the intended use. Vehicle states on the internal communication bus system at hand are

- the rms value of the stator phase current $i_{\mathrm{rms}} = \frac{\hat{i}}{\sqrt{2}}$,
- the electric power throughput $P_{\mathrm{e}} = \frac{3}{2}\hat{u}\hat{i}\cos(\varphi)$,
- the rotor speed $\dot{\theta}_{\mathrm{m}} = \dot{\theta}_{\mathrm{e}}/Z_{\mathrm{p}}$,
- an accurate estimation of the rotor torque T_{e},

at sampling frequencies of 1 kHz. In the above definition of the electric power, φ denotes the power factor angle and $\hat{i}$ denotes the peak value of the stator phase current. This choice of measurement data at relatively low sampling frequencies strongly limits the chance of identifying the parameter set (21). It is therefore necessary to make further assumptions on the model structure and to reduce the number of parameters to be identified.

First, it is assumed that the stator resitance R_{s} and the pole-pair number Z_{p} are known. These assumptions are widely-used in literature. The pole-pair number Z_{p} is often provided by the motor manufacturer or is otherwise identified from phase voltage and speed measurements. Since the stator terminals are easily accessible, the stator resitance R_{s} can be obtained from a resistance measurement. The parameter set to be identified is chosen as

$$p_{\mathrm{ident}} = \left\{\frac{L_{\mathrm{r}}}{M^2}, T_{\mathrm{r}}^{-1}, \frac{L_{\mathrm{r}}}{R_{\mathrm{fe}}}\right\}\,. \quad (22)$$

As will be shown shortly, the chosen parameter set (22) is sufficient to compute the stationary rms stator current and the electric power throughput in a restricted operating region. Although (22) can be identified without any a priori knowledge of the mutual inductance, an adequate estimation of M is required to retrieve the rotor parameters from (22). If in addition the stator inductance L_{s} needs to be identified, it is necessary to measure the rms stator phase voltage.

Second, in order to cope with the low sampling frequency, the proposed method makes use of a structural property referred to as differential flatness and the fact that the flat output is less dynamic than the system input and other internal states, Fliess et al. [1999]. In a previous study by Rolle and Sawodny [2019], it was shown that the rotor speed $\dot{\theta}_{\mathrm{e}}$, the rotor torque T_{e}, and the rotor flux linkage

λ'_{dr} are flat outputs of the model equations (15)-(17). As a consequence, an equivalent representation of the system states and inputs can be formulated as function of the flat outputs and their successive time derivatives

$$i_{\mathrm{ds}} = \frac{\lambda'_{\mathrm{dr}}}{M} + \frac{L_{\mathrm{r}}}{R'_{\mathrm{r}} M}\dot{\lambda}'_{\mathrm{dr}}\,, \tag{23}$$

$$i_{\mathrm{qs}} = \frac{2}{3}\frac{L_{\mathrm{r}}}{M}\frac{T_{\mathrm{e}}}{Z_{\mathrm{p}}\lambda'_{\mathrm{dr}}}\,, \tag{24}$$

$$u_{\mathrm{ds}} = \begin{array}{l}\frac{1}{M}\left(R_{\mathrm{s}}\lambda'_{\mathrm{dr}} - \left(\frac{4}{9}R'_{\mathrm{r}}\frac{T_{\mathrm{e}}^2}{Z_{\mathrm{p}}^2\lambda'^2_{\mathrm{dr}}} + \frac{2}{3}T_{\mathrm{e}}\dot{\theta}_{\mathrm{m}}\right)\frac{\sigma L_{\mathrm{s}}L_{\mathrm{r}}}{\lambda'_{\mathrm{dr}}} + \right. \\ \left.\left(\frac{R_{\mathrm{s}}}{R'_{\mathrm{r}}}L_{\mathrm{r}} + L_{\mathrm{s}}\right)\dot{\lambda}'_{\mathrm{dr}} + \sigma\frac{L_{\mathrm{s}}L_{\mathrm{r}}}{R'_{\mathrm{r}}}\ddot{\lambda}'_{\mathrm{dr}}\right)\end{array}\,, \tag{25}$$

$$u_{\mathrm{qs}} = \begin{array}{l}\frac{1}{M}\left(L_{\mathrm{s}}\dot{\theta}_{\mathrm{e}}\lambda'_{\mathrm{dr}} + \frac{2}{3}\left(L_{\mathrm{s}}R'_{\mathrm{r}} + L_{\mathrm{r}}R_{\mathrm{s}}\right)\frac{T_{\mathrm{e}}}{Z_{\mathrm{p}}\lambda'_{\mathrm{dr}}} + \right. \\ \left.\sigma L_{\mathrm{s}}\left(\frac{2}{3}L_{\mathrm{r}}\frac{\dot{T}_{\mathrm{e}}}{Z_{\mathrm{p}}\lambda'_{\mathrm{dr}}} + \frac{L_{\mathrm{r}}}{R'_{\mathrm{r}}}\dot{\theta}_{\mathrm{e}}\dot{\lambda}'_{\mathrm{dr}}\right)\right)\end{array}\,. \tag{26}$$

In stationary operating conditions with $\dot{\lambda}'_{\mathrm{dr}} = \ddot{\lambda}'_{\mathrm{dr}} = 0$ and $\dot{T}_{\mathrm{e}} = 0$, the rms square values of the stator phase current and phase voltage are given by

$$i^2_{\mathrm{rms,s}} = \frac{1}{2M^2}\left(\lambda'^2_{\mathrm{dr}} + \frac{4}{9}L_{\mathrm{r}}^2\frac{T_{\mathrm{e}}^2}{Z_{\mathrm{p}}^2\lambda'^2_{\mathrm{dr}}}\right), \tag{27}$$

$$u^2_{\mathrm{rms,s}} = \begin{array}{l}\frac{1}{2M^2}\left(\frac{4}{9}\left(\sigma L_{\mathrm{s}}L_{\mathrm{r}}\right)^2\left(\frac{4}{9}R'^2_{\mathrm{r}}\frac{T_{\mathrm{e}}^2}{Z_{\mathrm{p}}^2\lambda'^4_{\mathrm{dr}}} + \frac{4}{3}R'_{\mathrm{r}}\frac{T_{\mathrm{e}}\dot{\theta}_{\mathrm{m}}}{\lambda'^2_{\mathrm{dr}}} + \right.\right. \\ \frac{\left(L_{\mathrm{s}}R'_{\mathrm{r}}\right)^2 + 2R'_{\mathrm{r}}R_{\mathrm{s}}M^2 + \left(L_{\mathrm{r}}R_{\mathrm{s}}\right)^2}{\left(\sigma L_{\mathrm{s}}L_{\mathrm{r}}\right)^2} + \dot{\theta}_{\mathrm{e}}^2\Big)\frac{T_{\mathrm{e}}^2}{Z_{\mathrm{p}}^2\lambda'^2_{\mathrm{dr}}} + \\ \left.\left.\frac{4}{3}\left(L_{\mathrm{s}}^2R'_{\mathrm{r}} + M^2R_{\mathrm{s}}\right)T_{\mathrm{e}}\dot{\theta}_{\mathrm{m}} + \left(R_{\mathrm{s}}^2 + \left(L_{\mathrm{s}}\dot{\theta}_{\mathrm{e}}^2\right)\right)\lambda'^2_{\mathrm{dr}}\right)\right)\end{array} \tag{28}$$

and the electric power throughput, including core losses (20) is

$$P_{\mathrm{e}} = \frac{3}{2}\left(\frac{R_{\mathrm{s}}}{M^2} + \frac{\dot{\theta}_{\mathrm{e}}^2}{R_{\mathrm{fe}}}\right)\lambda'^2_{\mathrm{dr}} + \frac{2}{3}\left(R'_{\mathrm{r}} + \frac{L_{\mathrm{r}}^2}{M^2}R_{\mathrm{s}}\right)\frac{T_{\mathrm{e}}^2}{Z_{\mathrm{p}}^2\lambda'^2_{\mathrm{dr}}} + \dot{\theta}_{\mathrm{m}}T_{\mathrm{e}}\,. \tag{29}$$

As seen in (27) and (29), the rms stationary current and electric power only depend on the a priori known parameters and (22). The stator inductance L_{s} is solely used in the analytical expressions of the stator phase voltage which is interesting concerning the structural identifiability.

To derive a parameterized mapping from past IM states to the space of the modeled outputs, it is assumed that only stationary conditions are needed to represent the measured data. Choosing (27) and (29) as a baseline for this mapping, it is noted that the rotor flux linkage remains unknown. In a field oriented control, the rotor flux constitutes a degree of freedom, which can be used to optimize the IM drive efficiency. The existing literature on optimal setpoint control of IM is extensive and focuses on strategies that minimize the IM powerloss in every operating condition considering voltage and current constraints. It is referred to Quang and Dittrich [2015] for a comprehensive summary and for an exemplary use in vehicle applications see Windisch and Hofmann [2015].

The principle idea of the proposed identification method is based on the assumption that IM controls in vehicle applications make use of loss-minimizing control strategies or are able to determine the rotor flux empirically to guarantee the maximum possible IM efficiency. In both cases, this a priori knowledge of the operating strategy can be used to derive an estimation of the rotor flux as a function of the rotor speed and rotor torque according to

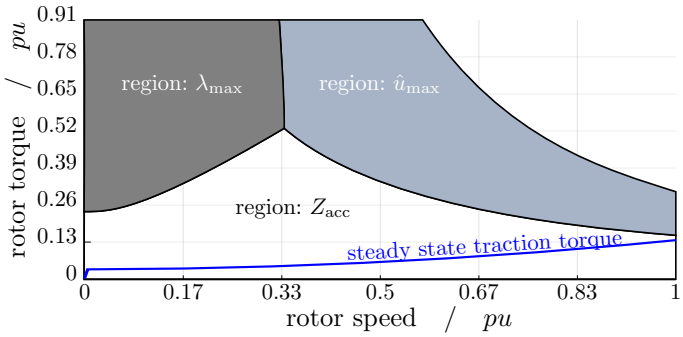

Fig. 2. Flux regions of loss minimizing field oriented control.

$$\lambda'^{\mathrm{acc}}_{\mathrm{dr}}\left(T_{\mathrm{e}}, \dot{\theta}_{\mathrm{m}}, p_{\mathrm{IM}}\right) = \underset{\lambda'_{\mathrm{dr}}}{\operatorname{argmin}}\; P_{\mathrm{e}}\left(T_{\mathrm{e}}, \dot{\theta}_{\mathrm{m}}, \lambda'_{\mathrm{dr}}, p_{\mathrm{IM}}\right) \tag{30}$$

$$= \left(\frac{4}{9}\frac{R'_{\mathrm{r}}M^2 + R_{\mathrm{s}}L_{\mathrm{r}}^2}{R_{\mathrm{s}} + \left(MZ_{\mathrm{p}}\dot{\theta}_{\mathrm{m}}\right)^2/R_{\mathrm{fe}}}\frac{T_{\mathrm{e}}^2}{Z_{\mathrm{p}}^2}\right)^{1/4}. \tag{31}$$

This estimation, however, is only valid in a specific region of the operating range and during acceleration and coasting

$$Z_{\mathrm{acc}} = \left\{(T_{\mathrm{e}}, \dot{\theta}_{\mathrm{m}})|\; \dot{\theta}_{\mathrm{m}}T_{\mathrm{e}} \geq 0\,,\; T_{\mathrm{e}} \leq T_{\mathrm{e}}^{\mathrm{ub}}\left(\dot{\theta}_{\mathrm{m}}\right)\right\}. \tag{32}$$

Figure 2 indicates this region for an exemple IM. The blue line represents the steady-state traction torque for a vehicle in the plane with a nominal vehicle mass as well as nominal drag and rolling resistance coefficients. The other two regions constitute the region in which the rotor flux is limited to its maximum value $\lambda_{\max}$ to avoid saturation, and the region in which the rotor flux is constrained by the dc-link voltage of the inverter and the maximum attainable phase voltage $\hat{u}_{\max}$ defined by (28). Consequently, the region $\hat{u}_{\max}$ expands with decreasing dc-link voltage at the cost of the maximum torque rating. Provided that measurements are restricted to a region in which (31) holds, inserting (31) in (27) and (29) yield

$$\left(i^{\mathrm{acc}}_{\mathrm{rms,s}}\right)^2 = \frac{1}{3M^2}\sqrt{\frac{T_{\mathrm{e}}^2}{Z_{\mathrm{p}}^2}}\left(\sqrt{\frac{R'_{\mathrm{r}}M^2 + R_{\mathrm{s}}L_{\mathrm{r}}^2}{R_{\mathrm{s}} + M^2\dot{\theta}_{\mathrm{e}}^2/R_{\mathrm{fe}}}} + L_{\mathrm{r}}^2\sqrt{\frac{R_{\mathrm{s}} + M^2\dot{\theta}_{\mathrm{e}}^2/R_{\mathrm{fe}}}{R'_{\mathrm{r}}M^2 + R_{\mathrm{s}}L_{\mathrm{r}}^2}}\right), \tag{33}$$

$$P^{\mathrm{acc}}_{\mathrm{e}} = \frac{2}{M^2}\sqrt{\left(R_{\mathrm{s}} + \frac{M^2\dot{\theta}_{\mathrm{e}}^2}{R_{\mathrm{fe}}}\right)\left(R'_{\mathrm{r}}M^2 + R_{\mathrm{s}}L_{\mathrm{r}}^2\right)\frac{T_{\mathrm{e}}^2}{Z_{\mathrm{p}}^2}} + \dot{\theta}_{\mathrm{m}}T_{\mathrm{e}}\,. \tag{34}$$

For regenerative breaking, it was observed that the field oriented control algorithm most likely follows a maximum torque per ampere strategy. Consequently an estimation for the rotor flux in the region of

$$Z_{\mathrm{brk}} = \left\{(T_{\mathrm{e}}, \dot{\theta}_{\mathrm{m}})|\; \dot{\theta}_{\mathrm{m}}T_{\mathrm{e}} < 0\,,\; T_{\mathrm{e}} \geq T_{\mathrm{e}}^{\mathrm{lb}}\left(\dot{\theta}_{\mathrm{m}}\right)\right\}, \tag{35}$$

is derived by employing

$$\lambda'^{\mathrm{brk}}_{\mathrm{dr}}(T_{\mathrm{e}}, p_{\mathrm{IM}}) = \underset{\lambda'_{\mathrm{dr}}}{\operatorname{argmin}}\; i^2_{\mathrm{rms,s}}(T_{\mathrm{e}}, \lambda'_{\mathrm{dr}}, p_{\mathrm{IM}}) = \left(\frac{4}{9}L_{\mathrm{r}}^2\frac{T_{\mathrm{e}}^2}{Z_{\mathrm{p}}^2}\right)^{1/4}, \tag{36}$$

to obtain

$$\left(i^{\mathrm{brk}}_{\mathrm{rms,s}}\right)^2 = \frac{2}{3}\frac{L_{\mathrm{r}}}{M^2}\sqrt{\frac{T_{\mathrm{e}}^2}{Z_{\mathrm{p}}^2}}. \tag{37}$$

Identification of the parameter set (22) is now done in three steps. Based on (33), (34) and (37) the parameterized mappings

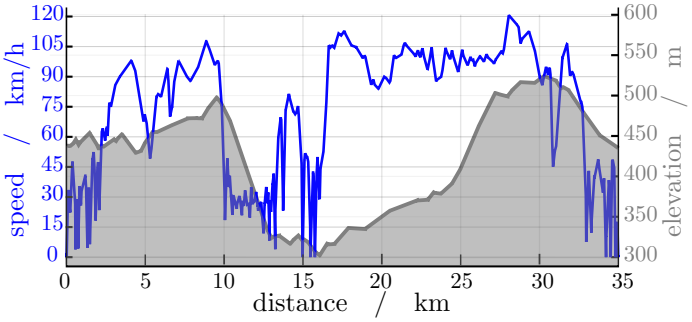

Fig. 3. Driving cycle (40 % freeway, 28 % federal highways, 28 % priority and main roads, 4 % lower priority roads).

$$y_1\left(i^{\mathrm{brk}}_{\mathrm{rms,s}}\right) = g_1(T_\mathrm{e}, p_\mathrm{ident})\,, \tag{38}$$

$$y_2\left(P^{\mathrm{acc}}_\mathrm{e}, i^{\mathrm{acc}}_{\mathrm{rms,s}}, T_\mathrm{e}, \dot\theta_\mathrm{m}\right) = g_2\left(P^{\mathrm{acc}}_\mathrm{e}, T_\mathrm{e}, \dot\theta_\mathrm{m}, p_\mathrm{ident}\right), \tag{39}$$

$$y_2\left(P^{\mathrm{acc}}_\mathrm{e}, i^{\mathrm{acc}}_{\mathrm{rms,s}}, T_\mathrm{e}, \dot\theta_\mathrm{m}\right) = g_3\left(T_\mathrm{e}, \dot\theta_\mathrm{m}, p_\mathrm{ident}\right), \tag{40}$$

are derived from

$$y_1 = \left(i^{\mathrm{brk}}_{\mathrm{rms,s}}\right)^2\,,\quad y_2 = \left(P^{\mathrm{acc}}_\mathrm{e} - \dot\theta_\mathrm{m} T_\mathrm{e}\right)\left(i^{\mathrm{acc}}_{\mathrm{rms,s}}\right)^2\,, \tag{41}$$

$$g_1 = \frac{2}{3}\frac{L_\mathrm{r}}{M^2}\sqrt{\frac{T_\mathrm{e}^2}{Z_\mathrm{p}^2}}\,, \tag{42}$$

$$g_2 = \frac{1}{6}\frac{\left(P^{\mathrm{acc}}_\mathrm{e} - \dot\theta_\mathrm{m} T_\mathrm{e}\right)^2}{T_\mathrm{r}^{-1}\left(\frac{L_\mathrm{r}}{M^2}\right)^{-1} + R_\mathrm{s}} + \frac{2}{3}\frac{T_\mathrm{e}^2}{Z_\mathrm{p}^2}\left(T_\mathrm{r}^{-1}\frac{L_\mathrm{r}}{M^2} + R_\mathrm{s}\left(\frac{L_\mathrm{r}}{M^2}\right)^2\right), \tag{43}$$

$$g_3 = \frac{2}{3}\frac{L_\mathrm{r}}{M^2}\left(T_\mathrm{r}^{-1} + 2\frac{L_\mathrm{r}}{M^2}R_\mathrm{s} + \frac{L_\mathrm{r}}{R_\mathrm{fe}}(Z_\mathrm{p}\dot\theta_\mathrm{m})^2\right)\frac{T_\mathrm{e}^2}{Z_\mathrm{p}^2}\,. \tag{44}$$

In the first step of the identification process, data

$$z^\mathrm{k} = \left(T^\mathrm{k}_\mathrm{e}, \dot\theta^\mathrm{k}_\mathrm{m}, P^\mathrm{k}_\mathrm{e}, i^\mathrm{k}_{\mathrm{rms,s}}\right) \tag{45}$$

are collected at discrete time instances $\mathrm{k} = 0(1)N-1$ in the region of (35). In order to comply with the assumption in (36), the lower bound on the rotor torque is chosen in a conservative manner (e.g. $T^{\mathrm{lb}}_\mathrm{e} = 0.2\,T_{\mathrm{e,min}}$). This data set is used to identify the rotor inductance by means of the least square error of,

$$\begin{aligned} p^* = \underset{p}{\operatorname{argmin}} \sum_{k=0}^{N-1}\left(y^k_{(.)} - g_{(.)}(\boldsymbol{z}^k, p)\right)^2 \\ s.t.\quad p^{\mathrm{lb}} \le p \le p^{\mathrm{ub}} \end{aligned}\,. \tag{46}$$

with parameter $p = L_\mathrm{r}/M^2$ and with g and y defined by (38). Analogously additional data are collected in the region of (32). In the second step, these data are used to identify the inverse of the rotor time constant T_r using the previously identified parameter together with (39) in (46). Eventually the ratio of rotor inductance and core loss resistance R_fe is identified based on (40). The nonlinear least-square problem (46) is solved using the Levenberg-Marquard algorithm. Bounds on the individual parameters can be chosen to restrict the feasible set, for example, to positive values.

4. EXPERIMENTAL STUDY

In the previous section several assumptions were made to derive parameterized mappings (38)-(40) from past IM

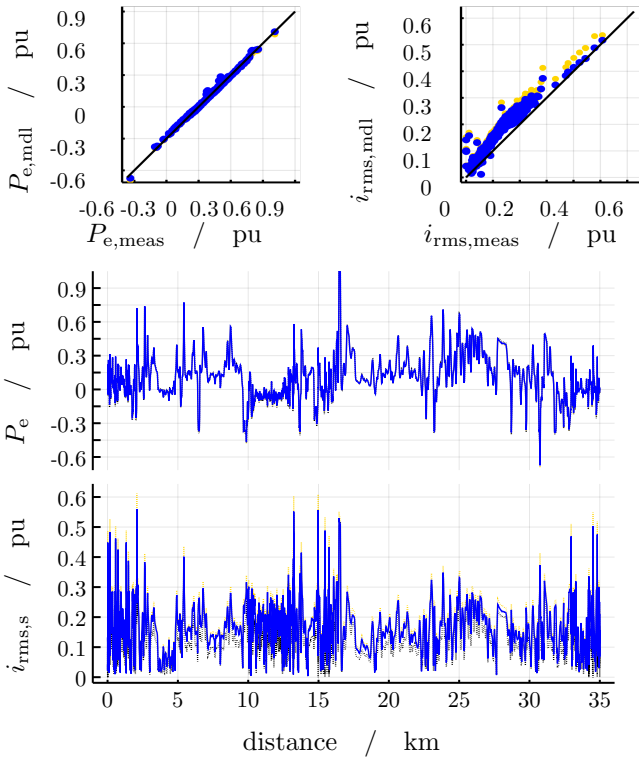

Fig. 4. Comparison of measured and modeled rms stator phase current i_rms and IM electric power throughput P_e (measurment - black; modeled - blue and yellow).

torque, speed, rms current, and electric power measurements to the space of the modeled outputs (41). These mappings are used to solve three problems of the form (46), one for each parameter in (22). In the following section, an experimental study is described, which addresses two questions:

- Are stationary operating conditions of the chosen model structure (23)-(26) sufficient to represent the observed behavior of a dynamic driving cycle?
- Does the premise of the IM field strategy allow for an accurate identification of the rotor parameters?

The vehicle used in this study is a battery-electric Mercedes-Benz EQC. The electric powertrain, features two 150 kW electric drive modules (EDM) on the front and rear axle. Available measurements at a sampling frequency of 1 kHz are listed in Section 3. A recorded real world driving cycle shown in Fig. 3 was driven on a *Daimler Powertrain Integration Center (AIZ)* test rig, onto which each wheel is connected to a high-power and high-precision electric drive to simulate realistic driving resistances and road conditions. Torque measurements on each axle were used to validate the torque estimate of the internal control system. During the test run, the driving mode was modified so that only one EDM was operating. The parameter set (21) for one of the IM was provided by the motor manufacturer. With the exception of the stator resistance R_s, the parameters of the second motor were unknown.

In the course of the experimental study, rotor parameters are identified following the proposed method in Section 3. The arbitrary initial guess of the rotor time constant was 1 sec, whereas the other parameters were set to zero. The

identified models (27) and (29) are modified so that the rotor flux linkage λ'_{dr} is also computed outside the region of $Z_{\mathrm{acc}} \cup Z_{\mathrm{brk}}$. For this purpose the maximum flux level can be identified by additional measurements at low speeds and the maximum rotor torque. Within the region of the maximum attainable voltage range, the flux level is determined by (28). This, however, requires an accurate estimation of the mutual inductance M and the stator self inductance L_{s} which were set equal to the provided manufacturer values. Consequently, the only remaining model inputs are the measured rotor torque and rotor speed.

The results obtained for the motor with the known parameter are presented in Fig. 4. Comparing the measurement of the rms stator current $i_{\mathrm{rms,meas}}$ and the electric power $P_{\mathrm{e,meas}}$ (indicated in black) with the modeled values of $i_{\mathrm{rms,mdl}}$ and $P_{\mathrm{e,mdl}}$ (indicated in blue), a high conformity between measurement and model is shown. Perhaps the most compelling finding of this comparison is that the assumption of stationary operating conditions is indeed sufficient to accurately resemble the observed behavior of a dynamic driving cycle. Additional test cycles, including generic cycles of speed changes at varying acceleration, confirm this finding as they led to similar results.

On the question concerning the parameter accuracy, the results obtained by the model using the manufacturer parameters are also displayed in Fig. 4 as yellow data points. While the electric power is well predicted, the original parameters lead to a slight difference when computing the rms current. In view of the linear dependency in (37), this overestimation results in an estimated rotor inductance which is 5 % less than the original manufacturer parameter, assuming that the provided value for mutual inductance is correct. This difference in the rotor inductance propagates to an increase of core loss resistance by 16 % and a decrease of the estimated rotor time constant by nearly 75 % (increase of R'_{r} by a factor of 2.8). While the rotor inductance and core loss resistance agree with the original parameter, the rotor resistance differs considerably. Since the provided parameters could not be confirmed by state-of-the-art identification methods, no further conclusion is made in the context of this study. For the purpose of performance analyses, however, the proposed models and identification method has proven to be simple and effective, as it was possible to obtain similar positive results for the second IM by iteratively adopting an initial guess for the unknown mutual inductance and the stator inductance.

5. CONCLUSION

This study set out to derive a system identification method for an induction motor loss model which can be used in motion control systems of battery electric vehicles. A new moddeling approach is proposed which is derived from the stationary equivalent flat system representation of the standard T-equivalent circuit and incorporates a priory knowledge of the vehicle specific field-oriented control strategy. Based on this formulation, model parameters are identified by minimizing the least-square error of the modeled outputs composed of the rms phase current and IM electric power. In an experimental study, the introduced model and proposed identification method have proven to accurately reproduce both of these electric system states for dynamic driving cycles. The most interesting and unanticipated finding of the experimental study is the high conformity of the stationary model in dynamic driving conditions. Consequently this study provides an alternative to state-of-the-art identification methods if required high frequency measurements of the stator phase voltage or current are hard to obtain. However it is important to note, that despite the promising results, the accuracy of the identification method could not be confirmed by standard identification procedures due to the shortage of available measurements and therefore should be investigated in further studies.

REFERENCES

Atkinson, D. J., Acarnley, P. P., Finch, J. W., Nov 1991. Observers for induction motor state and parameter estimation. IEEE Transactions on Industry Applications.

Besançon, G., Besançon-Voda, A., Bornard, G., Sep. 2001. A note on identifiability of induction motors. In: European Control Conference.

Castaldi, P., Tilli, A., May 2005. Parameter estimation of induction motor at standstill with magnetic flux monitoring. IEEE Transactions on Control Systems Technology.

Finken, T., Felden, M., Hameyer, K., Sep. 2008. Comparison and design of different electrical machine types regarding their applicability in hybrid electrical vehicles. International Conference on Electrical Machines.

Fliess, M., Lévine, J., Martin, P., Rouchon, P., May 1999. A Lie-Backlund approach to equivalence and flatness of nonlinear systems. IEEE Transactions on Automatic Control.

IEEE, Feb 2018. IEEE standard test procedure for polyphase induction motors and generators. IEEE Std 112-2017.

Krause, P. C., Thomas, C. H., Nov 1965. Simulation of symmetrical induction machinery. IEEE Transactions on Power Apparatus and Systems.

Krause, P. C., Wasynczuk, O., Sudhoff, S. D., Pekarek, S., 2013. Analysis of electric machinery and drive systems. John Wiley & Sons, Piscataway, NJ.

Lim, S., Nam, K., Jul 2004. Loss-minimising control scheme for induction motors. IEE Proceedings - Electric Power Applications.

Ljung, L., 2009. System identification: theory for the user, 2nd Edition. Prentice Hall, Upper Saddle River, NJ.

Pellegrino, G., Vagati, A., Boazzo, B., Guglielmi, P., Nov 2012. Comparison of induction and PM synchronous motor drives for EV application including design examples. IEEE Transactions on Industry Applications.

Quang, N. P., Dittrich, J., 2015. Optimal control of state variables and set points for im drives. In: Vector Control of Three-Phase AC Machines: System Development in the Practice. Springer Berlin Heidelberg.

Rolle, B., Sawodny, O., Sep 2019. Flatness based optimal control for induction machine drives. IFAC-PapersOnLine,8th IFAC Symposium on Mechatronic Systems.

Shaw, S. R., Leeb, S. B., Feb 1999. Identification of induction motor parameters from transient stator current measurements. IEEE Transactions on Industrial Electronics.

Toliyat, H. A., Levi, E., Raina, M., June 2003. A review of rfo induction motor parameter estimation techniques. IEEE Transactions on Energy Conversion.

Windisch, T., Hofmann, W., Nov 2015. Loss minimizing and saturation dependent control of induction machines in vehicle applications. Conference of the IEEE Industrial Electronics Society.

Yang, S., Ding, D., Li, X., Xie, Z., Zhang, X., Chang, L., Dec 2017. A novel online parameter estimation method for indirect field oriented induction motor drives. IEEE Transactions on Energy Conversion.

Zai, L., DeMarco, C. L., Lipo, T. A., Jan 1992. An extended kalman filter approach to rotor time constant measurement in pwm induction motor drives. IEEE Transactions on Industry Applications.